



1 GIS-based earthquake-triggered landslide susceptibility mapping 2 with an integrated weighted index model in Jiuzhaigou region of 3 Sichuan Province, China

4 Yaning Yi ^{1,2}, Zhijie Zhang ^{3,*}, Wanchang Zhang ^{1,*}, Qi Xu ⁴, Cai Deng ¹ and Qilun Li ^{1,2}

5 ¹Key Laboratory of Digital Earth Science, Institute of Remote Sensing and Digital Earth, Chinese Academy of Sciences,
6 Beijing 100094, China

7 ²University of Chinese Academy of Sciences, Beijing, 100049, China

8 ³Department of Geography, University of Connecticut, Storrs, CT, 06269, USA

9 ⁴Institute of Karst Geology, Chinese Academy of Geological Sciences, Guilin 541004, China

10 *Correspondence to:* Zhijie Zhang (zhijie.zhang@uconn.edu) and Wanchang Zhang (zhangwc@radi.ac.cn)

11 **Abstract.** A Ms 7.0 earthquake struck the Jiuzhaigou region of Sichuan Province, China at 21:19 pm on Tuesday, 8 August
12 2017, which triggered a large number of landslides. For mitigating the damages of earthquake-triggered landslides to
13 individuals and infrastructures of the earthquake affected region, a comprehensive landslide susceptibility mapping was
14 attempted with an integrated weighted index model by combining the frequency ratio and the analytical hierarchy process
15 approaches under GIS-based environment in the earthquake heavily attacked Zhangzha town of the Jiuzhaigou region. For
16 this purpose, a total number of 842 earthquake-triggered landslides were visually interpreted and located from Sentinel-2A
17 images acquired before and after the earthquake at first, and then the recognized landslides were randomly split into two
18 groups to establish the earthquake-triggered landslide inventory, among which 80 % of the landslides was used for training
19 the integrated model and the remaining 20 % for validation. Nine landslide controlling factors, namely slope, aspect,
20 elevation, lithology, distance from faults, distance from rivers, land-use/cover, normalized difference vegetation index and
21 peak ground acceleration, were considered with an integrated weighted index model for determination of the weighted index
22 through analysing their relationships with occurrence frequency ratios of landslides with analytical hierarchy process
23 approaches. Furthermore, an area under the curve approach was adopted to comprehensively evaluate the performance of the
24 integrated weighted index model, including the degree of model fit and model predictive capability. The results
25 demonstrated the reliability and feasibility of the integrated weighted index model in earthquake-triggered landslide
26 susceptibility mapping at regional scale. The generated map can be served as the scientific basis to mitigate hazards of the
27 earthquake-triggered landslides to individuals and infrastructures of the earthquake affected region.

28

29 **Keywords**

30 Earthquake-triggered landslide susceptibility mapping; An integrated weighted index model; Frequency ratio; Analytical
31 hierarchy process; The Jiuzhaigou region

32



1 Introduction

2 Recent natural disasters and their associated death tolls and financial costs have put mitigation of natural hazards at the
3 forefront of societal needs. Landslides are the most common natural disasters (geological hazards) that cause damages to
4 people's lives and property every year in many areas of the world (Saha et al., 2010; Su et al., 2015). Landslides are more
5 likely to occur when the slope becomes unstable. Slope instability can be caused by several factors, such as geological,
6 meteorological and anthropogenic factors, especially the earthquake and rainfall (Guzzetti et al., 2012; Sato et al., 2007).
7 On August 8, 2017, a catastrophic earthquake of magnitude 7.0 struck the Jiuzhaigou region of Sichuan Province, China.
8 The epicentre of this earthquake with a depth of 20 km was located latitude 33.20° N and longitude 103.82° E close to the
9 Jiuzhaigou National Nature Reserve, about 39 km West from the city of Jiuzhaigou. According to China Earthquake
10 Administration, this earthquake was caused by tectonic movement of an NW-SE-oriented left-lateral strike-slip fault (Wang
11 et al., 2018a). Although the intense rainfall was not observed after the earthquake, numerous landslides were triggered yet by
12 strong seismic vibration of ground (Zhao et al., 2018). Many tourists were trapped in the region due to numerous landslides
13 blocking the roads. Based on field investigation, most of these landslides were small-scale rock slides, rock falls and debris
14 slides (Fan et al., 2018; Zhao et al., 2018). As China Earthquake Administration reported, this earthquake caused 25 deaths
15 and 176,492 injured or affected (Lei et al., 2018; Wang et al., 2018b). Comprehensive earthquake-triggered landslide
16 susceptibility mapping in the earthquake affected area, therefore, is essential to mitigate landslide damages through the
17 proper prevention actions for the future. Over the last decades, many approaches for landslide susceptibility mapping were
18 proposed, among which the application of remote sensing associated with GIS modelling techniques became the most
19 popular and effective ones (Alexander, 2008; Carrara et al., 1991; Dai and Lee, 2002; Guzzetti et al., 1999; Lee, 2005;
20 Mantovani et al., 1996; Mansouri Daneshvar, 2014; Xu et al., 2012a).
21 The most commonly used methods for landslide susceptibility mapping include logistic regression (Ayalew and Yamagishi,
22 2005; Bai et al., 2010; Ozdemir and Altural, 2013), weights of evidence (Althuwaynee et al., 2012; Regmi et al., 2010),
23 analytical hierarchy process (AHP) (Kayastha et al., 2013; Komac, 2006; Mansouri Daneshvar, 2014; Yalcin, 2008),
24 frequency ratio (FR) (Guo et al., 2015; Li et al., 2017; Mohammady et al., 2012), support vector machine (SVM)
25 (Marjanović et al., 2011; Su et al., 2015), decision tree (Nefeslioglu et al., 2010; Saito et al., 2009) and artificial neural
26 network (ANN) (Conforti et al., 2014; Pradhan and Lee, 2009). These methods have been proved capable of mapping the
27 locations that are prone to landslides, however, some shortcomings yet exist in these methods, which reduce the efficiency of
28 these susceptibility methods when applied individually (Tien Bui et al., 2012; Umar et al., 2014). For example, the AHP can
29 be used to identify the mutual relationship between landslide controlling factors and the landslide susceptibility, but the
30 process and results mostly depend on the expert's knowledge, which are somehow subjective in practice (Youssef et al., 2015;
31 Zhang et al., 2016). The FR is capable of representing the influence of the categories of each controlling factor due to
32 landslide occurrences (Lee and Talib, 2005), however, the mutual relationship between the factors is mostly neglected, and
33 the same issue also exists in the modelled result. Logistic regression is good at analysing the relationships among the



1 landslide controlling factors but is not capable to evaluate the impact of the categories of each factor individually on
2 landslides (Umar et al., 2014). Fuzzy logic has also been employed in landslide susceptibility mapping, but the modelled
3 results largely rely on the expert's knowledge, which often leads to a high degree of uncertainty (Tilmant et al., 2002). In
4 addition, machine learning models (e.g. SVM, decision tree and ANN models) are very popular methods in landslide
5 analysis, nevertheless, heavy dependence of a very high-speed computer along with large amounts of training data needed
6 constrain their practical applications to some extent (Umar et al., 2014).

7 In addition, the combined approach has been gradually used for landslide susceptibility assessment (Ba et al., 2017; Boon et
8 al., 2015; Dehnavi et al., 2015; Kadavi et al., 2018; Pham et al., 2018; Shrestha et al., 2017; Umar et al., 2014; Youssef et al.,
9 2015). For instance, Umar et al. (Umar et al., 2014) used an ensemble method of FR and logistic regression to assess the
10 landslide susceptibility in West Sumatera Province, Indonesia, and the similar integrated method was also applied by
11 Youssef et al. (Youssef et al., 2015). Dehnavi et al. (Dehnavi et al., 2015) combined the step-wise weight assessment ratio
12 analysis method and adaptive neuro-fuzzy inference system to produce a landslide susceptibility map of Iran. Ba et al. (Ba et
13 al., 2017) proposed an improved information value model based on grey clustering for landslide susceptibility mapping in
14 Chongqing. Kadavi et al. (Kadavi et al., 2018) proposed a hybrid machine learning approach of AdaBoost, LogitBoost,
15 Multiclass Classifier, and Bagging models for spatial prediction of landslides. Although those studies suggested
16 effectiveness of the integrated method in some areas of the world, the universality and efficiency of the integrated method
17 were yet remained as an important issue to be confirmed in different regions of the world (Reichenbach et al., 2018).

18 The main purpose of this study was to apply an integrated weighted index model by combining FR and AHP for
19 susceptibility mapping of earthquake-triggered landslides. The integrated model is capable of evaluating the contribution of
20 each landslide controlling factor to landslide occurrence using FR method, meanwhile taking mutual relationships among
21 controlling factors into account by the use of AHP. Such integration is capable to generate a complete model that largely
22 restrains the shortcomings of these two individual methods and reduces the uncertainty and subjectivity resulted by the
23 utilization of individual method. The experiment site was selected at the Zhangzha town of Jiuzhaigou, a region seriously
24 affected by the Jiuzhaigou earthquake. An earthquake-triggered landslide susceptibility map was produced by using the
25 integrated weighted index model along with the remotely sensed information, a detailed validation analysis by using an area
26 under the curve approach was conducted to the generated susceptibility map of the study area for evaluating the reliability
27 and feasibility of the integrated model. This manuscript is structured as follows: Section 2 introduces the study area and the
28 basic information about the earthquake happened on August 8, 2017. Section 3 describes the data utilized and data preparing
29 procedures. Section 4 gives the detailed explanation about the integrated weighted index model. Section 5 presents the
30 results and discussions focusing on validations on the generated earthquake-triggered landslide susceptibility map of the
31 study area followed by the conclusions drawn in Section 6 at the end.



1 2 Study area

2 The study area with an area of about 1345.19 km², as shown in Fig. 1, is located in the Zhangzha town of Jiuzhaigou County
3 between 33.03° N – 33.35° N Latitude and 103.63° E – 104.05° E Longitude in the Min Shan Mountains on the north of the
4 Sichuan basin, eastern margin of the Tibetan Plateau. The geological conditions of this region are extremely complex. The
5 soluble carbonate rocks are widely distributed along with tufa deposition of karst developed, and regional tectonic
6 movements are intense here (Wang et al., 2018b). The topography of the region is characterized by alpine karst terrain where
7 the elevation varies from 1624 m to 4855 m above mean sea level. The Jiuzhaigou County belongs to a cold sub-humid and
8 cold semi-arid monsoon climate with the annual precipitation about 550 mm (Li et al., 2014). The geomorphology of the
9 study area is jointly formed by the climatic, geotectonic, lithological conditions under the effect of topography of the region.
10 Due to abundant recharge supply of groundwater in this region, many lakes and streams develop over extensive alpine karst
11 developed region, which favours the hill slope erosion processes, and results in frequent occurrence of rock slides, debris
12 flows, and rock falls there.

13 The Jiuzhaigou National Nature Reserve, approved as the UNESCO World Biosphere Reserve, is just located in the study
14 area. Many scenic spots in the Jiuzhaigou National Nature Reserve were destroyed in 2017 by the Jiuzhaigou earthquake, as
15 presented in Fig. 2(b), the Sparkling Lake was damaged. A significant number of small-scale landslides, as shown in Fig. 1,
16 were triggered by this earthquake along roads and river valley where many residents and infrastructures are located.
17 Landslides seriously threaten the anthropogenic activities, as well as tourist facilities of the region, as can be seen in Fig.
18 2(d), the S301 highway was severely obstructed by rock falls and rock slides, which drawn great attentions extensively.

19 3 Data

20 In order to map the landslide susceptibility of the study area, we designed and developed a spatial database with the help of
21 ArcGIS (version 10.2) software. This database contained two primary parts: (1) the landslide inventory dataset for
22 earthquake-triggered landslides; and (2) the datasets of background condition representing the landslide controlling factors.
23 The data layers used in the landslide susceptibility mapping were briefly described as presented in the Table 1.

24 3.1 Landslide inventory

25 Landslide inventory is essential for analysing the relationships between controlling factors and the landslide occurrences, and
26 also useful for assessing landslide hazard or risk on a regional scale (Pellicani and Spilotro, 2015). The Jiuzhaigou
27 earthquake on August 8, 2017 with a magnitude of 7.0 triggered numerous landslides in the study area. For deriving
28 landslide inventory containing detailed and reliable information on landslide distribution, location, etc., Sentinel-2A images
29 acquired on July 29, August 13 and September 7, 2017 were used to recognize and locate the earthquake-triggered landslides.
30 Sentinel-2A image has 13 spectral bands (from the blue to the shortwave infrared) with the spatial resolution of 10 m, 20 m
31 and 60 m, respectively. In this study, three visible bands (red, green, blue) with the spatial resolution of 10 m were adopted



1 to establish the image feature sets of earthquake-triggered landslides based on the visual interpretation of the landslide image
2 characteristics. With the aid of computer and GIS tools, the landslide information of the study area was extracted using on-
3 screen visual interpretation on pre- and post-earthquake Sentinel-2A images, as examples presented in Fig. 2. In order to
4 ensure the quality of visual interpretation, GF-1 images with spatial resolution of 2 m acquired on January 15, 2017, were
5 used to verify the results. Consequently, a total number of 842 earthquake-triggered landslides were recognized and
6 positioned. Smaller landslides were not included as they were not clear enough in visual features. We assumed that the
7 distribution of the earthquake-triggered landslides was reasonably accurate and complete at regional scale in order to make
8 the problem tractable. For earthquake-triggered landslide susceptibility mapping, the landslide inventory dataset was
9 randomly split into two groups, among which 80 % (673 landslides) of the recognized landslides was used for training the
10 integrated weighted index model and the remaining 20 % (169 landslides) for validation.

11 3.2 Landslide controlling factors

12 The occurrence of landslides is a consequence of geological, meteorological, anthropogenic and triggering factors,
13 commonly referred to as landslide controlling factors (Bai et al., 2010). Standard guidelines for choosing the optimal
14 landslide controlling factors are unavailable, but the scale of the analysis, the nature of the study area, the data availability
15 and the quasi-empirical and statistical criterions in literatures can be referenced (Romer and Ferentinou, 2016; Zhou et al.,
16 2016). In present study, slope, aspect, elevation, lithology, distance from faults, distance from rivers, land-use/cover (LULC),
17 normalized difference vegetation index (NDVI) and peak ground acceleration (PGA) were selected as the landslide
18 controlling factors, as shown in Fig. 3, for analysis.

19 Among all landslide controlling factors, slope, aspect and elevation have been recognized as the most important topographic
20 factors closely related to landslides (Ayalew and Yamagishi, 2005; Chalkias et al., 2016). Slope directly affects the velocity
21 of both surface and subsurface flows (Su et al., 2015). Pioneer studies suggested that landslides become possible once the
22 slope gradient is higher than 15° (Lee and Min, 2001). In the study area, the slopes were generally steep, with an average
23 slope angle of about 29.92°. Aspect, referred to the direction of slope faces, is related to the soil moisture, surface runoff and
24 vegetation growing conditions, which indirectly affects the landslide development (Zhang et al., 2016). The elevation, as the
25 measure of the land surface height, is a key factor determining gravitational potential energy of terrain and was often
26 considered in relevant studies (Conforti et al., 2014; Peng et al., 2014). In the study area, the rugged terrain makes the slope
27 very unstable. Topographic factors can be calculated with DEM. The DEM from SRTM database was used to extract slope
28 (0°–78°), aspect and elevation (1624–4855 m in the study area) in the study area.

29 Lithology is directly related to the slope stability, which plays an important role as one of landslide controlling factors. Ten
30 geological formation units including Quaternary (Q, Qh), Triassic (T1, T2, T3), Permian (P, P2), Carboniferous (C), and
31 Devonian (D) outcrop in the study area (Wang et al., 2018a). For the Jiuzhaigou earthquake, most landslides in the study
32 area occurred in the carboniferous formations which is mainly composed of metamorphic quartzite sandstones, limestone
33 and slate (Fan et al., 2018). In addition, the Permian limestone and Triassic sandstone also exhibited a large number of



1 landslides. The distances of a slope from faults as well as from the river channels are also important factors in terms of slope
2 stability. In addition, earthquake-triggered landslides usually are found in the vicinity of active faults. Hence, the distances of
3 a slope from geological tectonic zone were often taken into account in slope stability analysis. According to the China
4 Earthquake Administration, the epicentre of the Jiuzhaigou earthquake was located near the Minjiang, Tazang and Huya
5 faults. Some studies had revealed that this earthquake occurred along a previously unknown blind fault probably belonging
6 to a south branch of the Tazang fault or north part of the Huya fault (Fan et al., 2018). However, due to its great uncertainty,
7 this blind fault was not taken into account in the study area. Streams also have an impact on the slope stability because soil
8 water erosion is prone to take place next to the rivers on slopes. And the LULC map is one of controlling factors that pose
9 direct impact on the occurrence of landslides. For the Jiuzhaigou earthquake, most landslides in the study area occurred in
10 the wood land. In this study, the lithological data was obtained from the geological map at 1: 500,000 scale and was digitized
11 in ArcGIS for further analysis.

12 Vegetation coverage poses effect on soil water erosion, which indirectly affects the occurrence of landslides. NDVI, as the
13 measure of vegetation coverage, was usually adopted in landslide susceptibility analysis (Siqueira et al., 2015). The NDVI
14 was calculated from these individual measurements as follows:

$$15 \quad NDVI = \frac{DN_{NIR} - DN_R}{DN_{NIR} + DN_R}, \quad (1)$$

16 Where, DN_{NIR} stands for the spectral reflectance derived from the measured radiances in the near-infrared regions (NIR), and
17 DN_R stands for the spectral reflectance derived from the measured radiances in the visible (Red) regions.

18 In this study, the NDVI map was generated from the Landsat-8 image acquired on April 8, 2017 over the study area.

19 As an important dynamic factor, earthquake often triggers slope failures. Usually, the impact of earthquake on landslides was
20 measured and quantified by recording the absolute maximum amplitude of ground acceleration (PGA) (Chalkias et al., 2016).

21 The PGA map of the study area was downloaded from the USGS website (<https://www.usgs.gov>).

22 Landslide controlling factors, i.e., (a) slope, (b) aspect, (c) elevation, (d) lithology, (e) distance from faults, (f) distance from
23 rivers, (g) LULC, (h) NDVI, (i) PGA, as illustrated in Fig. 3, were generated as described above. To ensure the consistency
24 and easy process of these data, all factor layers were converted into raster data format (GeoTIFF) with an identical spatial
25 projection (WGS84 datum) and resampled to a resolution of 30 m by ENVI 5.3 and ArcGIS 10.2.

26 4 Methodology

27 In this study, an integrated weighted index model was developed as a complete landslide susceptibility model by combining
28 AHP and FR approaches. The assumption behind the integrated weighted index model was that future landslides will occur
29 under similar environmental conditions as historical landslides (Guzzetti et al., 1999; Pourghasemi and Rahmati, 2018), and
30 the susceptibility can be evaluated from the relationship between the controlling factors and the landslide occurrence area
31 (Zhu et al., 2014). In the present study, the integrated weighted index model was run through three general steps: (1)



1 determining the relative importance of landslide controlling factors using AHP method, (2) characterizing the relationships
2 between controlling factors and landslide locations using FR and GIS techniques, and (3) predicting landslide susceptibility
3 using weighted overlay analysis. The integrated model can assess the correlation between the controlling factors and also the
4 influence of each landslide controlling factor on landslide occurrence.

5 The integrated weighted index was calculated as follows:

$$6 \quad I = \sum_i^m (W_i \times FR_i), \quad (2)$$

7 Where, m stands for number of controlling factors, W_i is the weight of each controlling factor calculated by the AHP method,
8 FR_i is the FR value of the controlling factor calculated by the FR method.

9 4.1 Analytical hierarchy process (AHP)

10 The AHP method, developed by Saaty (Saaty, 1977), is an important multiple criteria decision-making method (Vaidya and
11 Kumar, 2006), which has been applied for landslide susceptibility assessment for many years (Akgun, 2012; Kayastha et al.,
12 2013; Komac, 2006; Pourghasemi et al., 2012; Yalcin, 2008).

13 For the AHP, a complex non-structural problem was broken into its component parameters which were considered as the
14 factors of this study. Then, the contribution of factors was converted into numerical values with the help of a pair-wise
15 comparison matrix generated through comparing the relative importance of each factor based on the expert's prior
16 experience and knowledge (Vargas, 1990). In addition, it also provided a methodology to judge the relative importance of
17 factors by scoring. When a factor is more important than another, the score varies between 1 and 9. Conversely, the score
18 varies between 1/2 and 1/9. The higher the score, the greater the importance of the factor. Finally, weights of factors were
19 determined in the process of a pair-wise comparison matrix using Python software, and the weights with the Consistency
20 Ratio (CR) less than 0.1 were accepted.

21 4.2 Frequency ratio (FR)

22 The FR method is one of the most widely used approaches to assess the landslide susceptibility at regional scale, which is
23 based on the observed spatial relationship between landslide locations and controlling factors (Poudyal et al., 2010). The
24 definition of FR is the ratio of the probability of the occurrence to the non-occurrence for given properties (Lee and Talib,
25 2005). The spatial relationship between landslides and controlling factors can be investigated through the FR method. The
26 average value of FR is 1 so that a value larger than one represents a higher correlation and those less than it, a lower
27 correlation (Romer and Ferentinou, 2016).

28 The FR value can be calculated as follows (Ghobadi et al., 2017):

$$29 \quad FR_i = \frac{N_{cell}(S_i)/N_{cell}(N_i)}{\sum N_{cell}(S_i)/\sum N_{cell}(N_i)}, \quad (3)$$



1 Where, $N_{cell}(S_i)$ represents number of grid cells recognized as landslides in class i , and $N_{cell}(N_i)$ represents total number
2 of grid cells belonging to class i in the whole area; while $\sum N_{cell}(S_i)$ stands for the total number of grid cells recognized as
3 landslides in the whole area, and $\sum N_{cell}(N_i)$ represents total number of grid cells in the whole area.

4 **5 Results and discussions**

5 **5.1 Landslide susceptibility mapping**

6 In this study, the relative importance of landslide controlling factors was determined from the prior experience and
7 knowledge of experts. Since the knowledge source varies from person to person, the best judgment always comes from an
8 individual who has good expertise (Ayalew et al., 2004). To find the appropriate correlation between controlling factors, we
9 investigated some related literatures (Shahabi and Hashim, 2015; Xu et al., 2012b; Zhang et al., 2016) and consulted with
10 some professional experts. Finally, the pair-wise comparison matrix was determined by means of discussion (Table 2) and a
11 general consensus achieved by experts. The AHP method was used to assign the weights for each controlling factor (Table 2).
12 In the Table 2, the weights for the nine controlling factors were estimated as follows: slope - 0.222, aspect - 0.043, elevation
13 - 0.058, lithology - 0.116, distance from faults - 0.197, distance from rivers - 0.080, LULC - 0.083, NDVI - 0.043 and PGA -
14 0.158. The Consistency Ratio was 0.017, which showed that the pair-wise comparison matrix satisfied the consistency
15 requirement. The higher the weight, the more impacts on landslide occurrence could be expected. The weight of slope was
16 highest, implying the most significant influence of slope on the landslide occurrence, and the weights of aspect and NDVI
17 were the lowest, which indicated that these two factors played the least role in the landslide occurrence.

18 Thus, the FR was considered as a measure for the spatial relationship between landslides and controlling factors. Through
19 analysing the relationship between each controlling factor and the landslide occurrence, the FR values were calculated by
20 using the Eq. (3) (as shown in Table 3). The higher the FR was, the closer the relationship between the landslide controlling
21 factor and the landslide occurrence would be. In the term of the relationship between landslide occurrence and slope,
22 landslides mostly occurred in the slope ranging from 40° to 60° . For the elevation, landslides mostly occurred below the
23 elevation of 3400 m, which implied that the probability of landslide occurrence was higher in moderate steep mountainous
24 region. In terms of the aspect, the FR value was very high for the class of E, N, SE and NE, and it was lowest for the class of
25 Flat. For the lithology, the highest FR value was achieved for Permian System which influenced the landslide occurrence.
26 For the factor of distance from faults, the highest FR value belonged to the area higher than 2000 m. The distance from rivers
27 with the highest FR value for frequent landslide occurrence was found usually between 0 and 600 m, and landslides mostly
28 occurred in the region with low vegetation cover of less NDVI value. In the case of PGA, the value of 0.26 g had the highest
29 FR value, which indicated the significant influence of the earthquake on the landslide occurrence. In general, our results
30 were basically consistent with the previous study (Fan et al., 2018), which found that most of the landslides mainly occurred
31 in proximity of rivers and the epicentre, with an elevation of 2600 m to 3200 m and a slope of 35° to 55° .



1 Finally, the weighted index was calculated by using the Eq. (2). The landslide susceptibility map of study area was generated
2 by using Weighted Overlay Analysis tool of ArcGIS, and the study area was classified into seven categories of landslide
3 susceptibility levels as presented in Fig. 4: very high, high, relatively high, moderate, relatively low, low and very low by
4 using Natural Breaks (Jenks) method with ArcGIS, respectively.

5 According to the landslide susceptibility map, the location close to the epicentre and rivers was classified as the most
6 susceptible areas for landslides, and the high and very high landslide susceptible areas mostly located in the middle central
7 mountainous region accounting for 10.99 % of the study area. The low and very low susceptibility areas far from the
8 epicentre and less affected by the earthquake, mainly distributed in the North and South-West parts of the study area,
9 accounting for approximately 35.06 % of the study area. Generally, the landslide susceptibility map generated by the
10 integrated weighted index model can reflect the potential area of the landslide occurrence in the study area.

11 5.2 Validations

12 For landslide susceptibility mapping, detailed validation of the modelled results is essential. A simple procedure of
13 validation can make a comprehensive and reasonable interpretation of the future landslide hazard (Chung and Fabbri, 2003).
14 In this study, operating characteristics curve (ROC) approach (Brenning, 2005; Bui et al., 2016) was adopted to evaluate the
15 performance of the integrated weighted index model, including the degree of model fit and model predictive capability. The
16 ROC curve was obtained by calculating the area under the curve (AUC) and the AUC value varied from 0.5 to 1.0 (Umar et
17 al., 2014). The AUC value of 1.0 implied a perfect performance of the model, whereas a value close to 0.5 indicated that the
18 model performed not so well. To assess the fitting performance of the integrated weighted index model, five sub-datasets
19 containing 20 %, 40 %, 60 %, 80 % and 100 % of training dataset (i.e., 673 landslides) respectively, were used to obtain the
20 fitting curves (Fig. 5(a)). Figure 5(a) shows a quantitative measure of the ability of integrated weighted index model to
21 describe the known distribution of landslides. The AUC values of five sub-datasets were 82.57 %, 84.52 %, 84.99 %, 86.08 %
22 and 85.65 %, respectively, which suggested the effective fitting capability of the integrated weighted index model developed
23 in this study.

24 To investigate the prediction performance of the integrated weighted index model, we also adopted five sub-datasets
25 containing 20 %, 40 %, 60 %, 80 % and 100 % of validation dataset (i.e., 169 landslides) respectively, to estimate the
26 prediction rates. Note that the validation dataset (i.e., 20 % of the landslide inventory dataset) was not used in the training
27 process. The AUC values of five sub-datasets, as presented in Fig. 5(b), were 78.71 %, 81.66 %, 84.27 %, 86.09 % and
28 87.16 %, respectively. With the increase of input data, the performance of the integrated weighted index model was
29 significantly improved, which indicated a reliable predicting capability of the integrated weighted index model adopted in
30 this study.

31 In addition, the landslide density distribution of each susceptibility level was computed by associating landslides with the
32 classified landslide susceptibility map (as shown in Table 4). There was a clear trend that the increase in the level of
33 landslide susceptibility was highly correlated with the density of landslides. The high and very high susceptibility levels had



1 the significant high landslide density values, while the low susceptibility categories were just the opposite, which also
2 implied the effectiveness of the generated landslide susceptibility map of study area.

3 **5.3 Discussions**

4 Landslide susceptibility is defined as the likelihood of landslides occurring in an area under local environmental conditions
5 (Fell et al., 2008; Reichenbach et al., 2018). The susceptibility can be evaluated from the relationship between the
6 environmental conditions and previous landslides (Zhu et al., 2014). There are numerous methods that have been proposed to
7 model this relationship. The main purpose of this study was to assess the spatial probability of landslide occurrences by
8 using an integrated weighted index model in association with the utilization of FR and AHP approaches to generate an
9 earthquake-triggered landslide susceptibility map. To achieve this objective, nine controlling factors (slope, aspect, elevation,
10 lithology, distance from faults, and distance from rivers, LULC, NDVI and PGA) were taken into consideration.

11 The FR is a data-driven statistical approach which can derive spatial relationship between landslide locations and controlling
12 factors. However, the FR method does not consider the mutual relationships between controlling factors. The AHP method is
13 an important multiple criteria decision-making method, which can overcome this shortcoming. To some extent, the
14 integrated method preserves the advantages of FR and AHP methods and restrains their weak points. Some similar studies
15 have also pointed it out (Reichenbach et al., 2018; Youssef et al., 2015; Zhou et al., 2016).

16 The implementation of the integrated weighted index model revealed that landslide susceptibility levels were basically
17 consistent with the distribution of earthquake-triggered landslides. The high susceptibility areas were concentrated in the
18 central mountainous region close to the epicentre of the earthquake of the study area, which indicated the significant
19 influence of the Jiuzhaigou earthquake on the landslide occurrence. From the landslide susceptibility map, the “very high”
20 and “high” susceptibility areas covered a significant part of the study area (10.99 % of the whole area) and most of the
21 Jiuzhaigou National Nature Reserve was classified as the most landslide susceptible areas.

22 Even though, some limitations yet existed in the proposed method. Firstly, the accuracy of FR method is highly depended on
23 the quality of dataset, especially the landslide inventory. Nevertheless, the landslide inventory is generally incomplete (Fell
24 et al., 2008), and is affected by many factors, such as the quality and scale of remote sensing images, the tectonic setting
25 complexity of study area, and the expertise of the interpreter involved (Malamud et al., 2004). In this study, we mainly
26 focused on the interpretation of earthquake-triggered landslides. We didn’t accurately identify the landslides before the
27 Jiuzhaigou earthquake due to the limitations of historical images, and smaller landslides were also not completely identified.
28 Future work should focus on the preparation of more detailed landslide inventories. Secondly, in this study, as the proposed
29 method was applied to medium-scale datasets, the results may not be suitable for specific analysis of large or detailed scale.
30 At large or detailed scales, more detailed landslide inventory dataset and controlling factor layers were required.
31 Additionally, the assumption behind much of the landslide susceptibility mapping is that future landslides will occur under
32 similar environmental conditions as historical landslides (Guzzetti et al., 1999; Pourghasemi and Rahmati, 2018). However,
33 results obtained in the past environmental conditions are not a guarantee for the future (Guzzetti et al., 2005). The



1 susceptibility results need to be adapted as soon as environmental conditions or their causal relationships obviously change
2 in the future, such as urban sprawl (van Westen et al., 2008). Despite its limitations, the integrated method can generate a
3 reliable landslide susceptibility map at regional scale which can provide the scientific basis for reconstruction of tourism
4 facilities, regional disaster management etc.

5 **6 Conclusions**

6 Earthquake is one of the dynamic causes in landslide occurrence. Earthquake-triggered landslides can cause extensive and
7 significant damages to both lives and properties. In this study, given the main motivation to adopt an integrated weighted
8 index model based on FR and AHP methods for earthquake-triggered landslide susceptibility mapping at the Zhangzha town
9 of the Jiuzhaigou County where a Ms 7.0 earthquake struck on Tuesday, 8 August 2017, nine factors such as slope, aspect,
10 elevation, lithology, distance from faults, distance from rivers, LULC, NDVI and PGA as landslide controlling factors were
11 adopted in the integrated weighted index model for generating the landslide susceptibility map of the study area with
12 reclassification of seven levels of landslide susceptibility areas within a GIS environment. The ROC approach was used to
13 comprehensively evaluate the performance of the integrated weighted index model, including the degree of model fit and
14 model predictive capability. The results demonstrated the reliability and feasibility of the integrated weighted index model in
15 landslide susceptibility mapping at regional scale.

16 Even some limitations do exist, the integrated weighted index model can generate a reliable landslide susceptibility map at
17 regional scale that is useful for serving the scientific basis for disaster mitigation and management. Furthermore, the
18 integration of some machine learning techniques should be taken into account in the integrated weighted index model for
19 advancement in future studies.

20 **Acknowledgments**

21 This study was supported by the National Key Research and Development Program of China, Grant No. 2016YFB0502502
22 and No. 2016YFA0602302. We would like to thank reviewers for their valuable suggestions and comments.

23 **References**

- 24 Akgun, A.: A comparison of landslide susceptibility maps produced by logistic regression, multi-criteria decision, and
25 likelihood ratio methods: a case study at İzmir, Turkey, *Landslides*, 9, 93-106, doi: 10.1007/s10346-011-0283-7, 2012.
26 Alexander, D. E.: A brief survey of GIS in mass-movement studies, with reflections on theory and methods, *Geomorphology*,
27 94, 261-267, doi: 10.1016/j.geomorph.2006.09.022, 2008.



- 1 Althuwaynee, O. F., Pradhan, B., and Lee, S.: Application of an evidential belief function model in landslide susceptibility
2 mapping, *Computers & Geosciences*, 44, 120-135, doi: 10.1016/j.cageo.2012.03.003, 2012.
- 3 Ayalew, L., Yamagishi, H., and Ugawa, N.: Landslide susceptibility mapping using GIS-based weighted linear combination,
4 the case in Tsugawa area of Agano River, Niigata Prefecture, Japan, *Landslides*, 1, 73-81, doi: 10.1007/s10346-003-0006-9,
5 2004.
- 6 Ayalew, L., and Yamagishi, H.: The application of GIS-based logistic regression for landslide susceptibility mapping in the
7 Kakuda-Yahiko Mountains, Central Japan, *Geomorphology*, 65, 15-31, doi: 10.1016/j.geomorph.2004.06.010, 2005.
- 8 Ba, Q., Chen, Y., Deng, S., Wu, Q., Yang, J., and Zhang, J.: An Improved Information Value Model Based on Gray
9 Clustering for Landslide Susceptibility Mapping, *ISPRS International Journal of Geo-Information*, 6, doi:
10 10.3390/ijgi6010018, 2017.
- 11 Bai, S.-B., Wang, J., Lü, G.-N., Zhou, P.-G., Hou, S.-S., and Xu, S.-N.: GIS-based logistic regression for landslide
12 susceptibility mapping of the Zhongxian segment in the Three Gorges area, China, *Geomorphology*, 115, 23-31, doi:
13 10.1016/j.geomorph.2009.09.025, 2010.
- 14 Boon, D. P., Chambers, J. E., Hobbs, P. R. N., Kirkham, M., Merritt, A. J., Dashwood, C., Pennington, C., and Wilby, P. R.:
15 A combined geomorphological and geophysical approach to characterising relict landslide hazard on the Jurassic
16 Escarpments of Great Britain, *Geomorphology*, 248, 296-310, doi: 10.1016/j.geomorph.2015.07.005, 2015.
- 17 Brenning, A.: Spatial prediction models for landslide hazards: review, comparison and evaluation, *Nat Hazard Earth Sys*, 5,
18 853-862, doi: 10.5194/nhess-5-853-2005, 2005.
- 19 Bui, D. T., Tuan, T. A., Klempe, H., Pradhan, B., and Revhaug, I.: Spatial prediction models for shallow landslide hazards: a
20 comparative assessment of the efficacy of support vector machines, artificial neural networks, kernel logistic regression, and
21 logistic model tree, *Landslides*, 13, 361-378, doi: 10.1007/s10346-015-0557-6, 2016.
- 22 Carrara, A., Cardinali, M., Detti, R., Guzzetti, F., Pasqui, V., and Reichenbach, P.: Gis Techniques and Statistical-Models in
23 Evaluating Landslide Hazard, *Earth Surf Proc Land*, 16, 427-445, doi: 10.1002/esp.3290160505, 1991.
- 24 Chalkias, C., Polykretis, C., Ferentinou, M., and Karymbalis, E.: Integrating Expert Knowledge with Statistical Analysis for
25 Landslide Susceptibility Assessment at Regional Scale, *Geosciences*, 6, 14, doi: 10.3390/geosciences6010014, 2016.
- 26 Chung, C. J. F., and Fabbri, A. G.: Validation of spatial prediction models for landslide hazard mapping, *Nat Hazards*, 30,
27 451-472, doi: 10.1023/B:Nhaz.0000007172.62651.2b, 2003.
- 28 Conforti, M., Pascale, S., Robustelli, G., and Sdao, F.: Evaluation of prediction capability of the artificial neural networks for
29 mapping landslide susceptibility in the Turbolo River catchment (northern Calabria, Italy), *Catena*, 113, 236-250, doi:
30 10.1016/j.catena.2013.08.006, 2014.
- 31 Dai, F. C., and Lee, C. F.: Landslide characteristics and, slope instability modeling using GIS, Lantau Island, Hong Kong,
32 *Geomorphology*, 42, 213-228, doi: 10.1016/S0169-555x(01)00087-3, 2002.



- 1 Dehnavi, A., Aghdam, I. N., Pradhan, B., and Morshed Varzandeh, M. H.: A new hybrid model using step-wise weight
2 assessment ratio analysis (SWARA) technique and adaptive neuro-fuzzy inference system (ANFIS) for regional landslide
3 hazard assessment in Iran, *Catena*, 135, 122-148, doi: 10.1016/j.catena.2015.07.020, 2015.
- 4 Fan, X., Scaringi, G., Xu, Q., Zhan, W., Dai, L., Li, Y., Pei, X., Yang, Q., and Huang, R.: Coseismic landslides triggered by
5 the 8th August 2017 Ms 7.0 Jiuzhaigou earthquake (Sichuan, China): factors controlling their spatial distribution and
6 implications for the seismogenic blind fault identification, *Landslides*, 15, 967-983, doi: 10.1007/s10346-018-0960-x, 2018.
- 7 Fell, R., Corominas, J., Bonnard, C., Cascini, L., Leroi, E., and Savage, W. Z.: Guidelines for landslide susceptibility, hazard
8 and risk zoning for land use planning, *Engineering Geology*, 102, 85-98, doi: 10.1016/j.enggeo.2008.03.022, 2008.
- 9 Ghobadi, M. H., Nouri, M., Saedi, B., Jalali, S. H., and Pirouzinajad, N.: The performance evaluation of information value,
10 density area, LNRF, and frequency ratio methods for landslide zonation at Miandarband area, Kermanshah Province, Iran,
11 *Arabian Journal of Geosciences*, 10, doi: 10.1007/s12517-017-3202-y, 2017.
- 12 Guo, C., Montgomery, D. R., Zhang, Y., Wang, K., and Yang, Z.: Quantitative assessment of landslide susceptibility along
13 the Xianshuihe fault zone, Tibetan Plateau, China, *Geomorphology*, 248, 93-110, doi: 10.1016/j.geomorph.2015.07.012,
14 2015.
- 15 Guzzetti, F., Carrara, A., Cardinali, M., and Reichenbach, P.: Landslide hazard evaluation: a review of current techniques
16 and their application in a multi-scale study, Central Italy, *Geomorphology*, 31, 181-216, doi: 10.1016/S0169-
17 555x(99)00078-1, 1999.
- 18 Guzzetti, F., Reichenbach, P., Cardinali, M., Galli, M., and Ardizzone, F.: Probabilistic landslide hazard assessment at the
19 basin scale, *Geomorphology*, 72, 272-299, doi: 10.1016/j.geomorph.2005.06.002, 2005.
- 20 Guzzetti, F., Mondini, A. C., Cardinali, M., Fiorucci, F., Santangelo, M., and Chang, K. T.: Landslide inventory maps: New
21 tools for an old problem, *Earth-Sci Rev*, 112, 42-66, doi: 10.1016/j.earscirev.2012.02.001, 2012.
- 22 Kadavi, P., Lee, C.-W., and Lee, S.: Application of Ensemble-Based Machine Learning Models to Landslide Susceptibility
23 Mapping, *Remote Sensing*, 10, doi: 10.3390/rs10081252, 2018.
- 24 Kayastha, P., Dhital, M. R., and De Smedt, F.: Application of the analytical hierarchy process (AHP) for landslide
25 susceptibility mapping: A case study from the Tinau watershed, west Nepal, *Computers & Geosciences*, 52, 398-408, doi:
26 10.1016/j.cageo.2012.11.003, 2013.
- 27 Komac, M.: A landslide susceptibility model using the Analytical Hierarchy Process method and multivariate statistics in
28 perialpine Slovenia, *Geomorphology*, 74, 17-28, doi: 10.1016/j.geomorph.2005.07.005, 2006.
- 29 Lee, S., and Min, K.: Statistical analysis of landslide susceptibility at Yongin, Korea, *Environmental Geology*, 40, 1095-
30 1113, doi: 10.1007/s002540100310, 2001.
- 31 Lee, S.: Application of logistic regression model and its validation for landslide susceptibility mapping using GIS and
32 remote sensing data, *International Journal of Remote Sensing*, 26, 1477-1491, doi: 10.1080/01431160412331331012, 2005.
- 33 Lee, S., and Talib, J. A.: Probabilistic landslide susceptibility and factor effect analysis, *Environmental Geology*, 47, 982-
34 990, doi: 10.1007/s00254-005-1228-z, 2005.



- 1 Lei, H., Wang, X., Hou, H., Su, L., Yu, D., and Wang, H.: The earthquake in Jiuzhaigou County of Northern Sichuan, China
- 2 on August 8, 2017, *Natural Hazards*, 90, 1021-1030, doi: 10.1007/s11069-017-3064-3, 2018.
- 3 Li, L., Lan, H., Guo, C., Zhang, Y., Li, Q., and Wu, Y.: A modified frequency ratio method for landslide susceptibility
- 4 assessment, *Landslides*, 14, 727-741, doi: 10.1007/s10346-016-0771-x, 2017.
- 5 Li, S., Hu, X., Tang, Y., Huang, C., and Xiao, W.: Changes in lacustrine environment due to anthropogenic activities over
- 6 240 years in Jiuzhaigou National Nature Reserve, southwest China, *Quaternary International*, 349, 367-375, doi:
- 7 10.1016/j.quaint.2014.07.069, 2014.
- 8 Malamud, B. D., Turcotte, D. L., Guzzetti, F., and Reichenbach, P.: Landslide inventories and their statistical properties,
- 9 *Earth Surf Proc Land*, 29, 687-711, doi: 10.1002/esq.1064, 2004.
- 10 Mansouri Daneshvar, M. R.: Landslide susceptibility zonation using analytical hierarchy process and GIS for the Bojnurd
- 11 region, northeast of Iran, *Landslides*, 11, 1079-1091, doi: 10.1007/s10346-013-0458-5, 2014.
- 12 Mantovani, F., Soeters, R., and Van Westen, C. J.: Remote sensing techniques for landslide studies and hazard zonation in
- 13 Europe, *Geomorphology*, 15, 213-225, doi: 10.1016/0169-555x(95)00071-C, 1996.
- 14 Marjanović, M., Kovačević, M., Bajat, B., and Voženilek, V.: Landslide susceptibility assessment using SVM machine
- 15 learning algorithm, *Engineering Geology*, 123, 225-234, doi: 10.1016/j.enggeo.2011.09.006, 2011.
- 16 Mohammady, M., Pourghasemi, H. R., and Pradhan, B.: Landslide susceptibility mapping at Golestan Province, Iran: A
- 17 comparison between frequency ratio, Dempster-Shafer, and weights-of-evidence models, *Journal of Asian Earth Sciences*,
- 18 61, 221-236, doi: 10.1016/j.jseaes.2012.10.005, 2012.
- 19 Nefeslioglu, H. A., Sezer, E., Gokceoglu, C., Bozkir, A. S., and Duman, T. Y.: Assessment of Landslide Susceptibility by
- 20 Decision Trees in the Metropolitan Area of Istanbul, Turkey, *Mathematical Problems in Engineering*, 2010, 1-15, doi:
- 21 10.1155/2010/901095, 2010.
- 22 Ozdemir, A., and Altural, T.: A comparative study of frequency ratio, weights of evidence and logistic regression methods
- 23 for landslide susceptibility mapping: Sultan Mountains, SW Turkey, *Journal of Asian Earth Sciences*, 64, 180-197, doi:
- 24 10.1016/j.jseaes.2012.12.014, 2013.
- 25 Pellicani, R., and Spilotro, G.: Evaluating the quality of landslide inventory maps: comparison between archive and surveyed
- 26 inventories for the Daunia region (Apulia, Southern Italy), *B Eng Geol Environ*, 74, 357-367, doi: 10.1007/s10064-014-
- 27 0639-z, 2015.
- 28 Peng, L., Niu, R., Huang, B., Wu, X., Zhao, Y., and Ye, R.: Landslide susceptibility mapping based on rough set theory and
- 29 support vector machines: A case of the Three Gorges area, China, *Geomorphology*, 204, 287-301, doi:
- 30 10.1016/j.geomorph.2013.08.013, 2014.
- 31 Pham, B. T., Prakash, I., and Bui, D. T.: Spatial prediction of landslides using a hybrid machine learning approach based on
- 32 Random Subspace and Classification and Regression Trees, *Geomorphology*, 303, 256-270, doi:
- 33 10.1016/j.geomorph.2017.12.008, 2018.



- 1 Poudyal, C. P., Chang, C., Oh, H.-J., and Lee, S.: Landslide susceptibility maps comparing frequency ratio and artificial
2 neural networks: a case study from the Nepal Himalaya, *Environmental Earth Sciences*, 61, 1049-1064, doi:
3 10.1007/s12665-009-0426-5, 2010.
- 4 Pourghasemi, H. R., Pradhan, B., and Gokceoglu, C.: Application of fuzzy logic and analytical hierarchy process (AHP) to
5 landslide susceptibility mapping at Haraz watershed, Iran, *Nat Hazards*, 63, 965-996, doi: 10.1007/s11069-012-0217-2, 2012.
- 6 Pourghasemi, H. R., and Rahmati, O.: Prediction of the landslide susceptibility: Which algorithm, which precision?, *Catena*,
7 162, 177-192, doi: 10.1016/j.catena.2017.11.022, 2018.
- 8 Pradhan, B., and Lee, S.: Regional landslide susceptibility analysis using back-propagation neural network model at
9 Cameron Highland, Malaysia, *Landslides*, 7, 13-30, doi: 10.1007/s10346-009-0183-2, 2009.
- 10 Regmi, N. R., Giardino, J. R., and Vitek, J. D.: Modeling susceptibility to landslides using the weight of evidence approach:
11 Western Colorado, USA, *Geomorphology*, 115, 172-187, doi: 10.1016/j.geomorph.2009.10.002, 2010.
- 12 Reichenbach, P., Rossi, M., Malamud, B. D., Mihir, M., and Guzzetti, F.: A review of statistically-based landslide
13 susceptibility models, *Earth-Sci Rev*, 180, 60-91, doi: 10.1016/j.earscirev.2018.03.001, 2018.
- 14 Romer, C., and Ferentinou, M.: Shallow landslide susceptibility assessment in a semiarid environment — A Quaternary
15 catchment of KwaZulu-Natal, South Africa, *Engineering Geology*, 201, 29-44, doi: 10.1016/j.enggeo.2015.12.013, 2016.
- 16 Saaty, T. L.: A scaling method for priorities in hierarchical structures, *Journal of Mathematical Psychology*, 15, 234-281, doi:
17 10.1016/0022-2496(77)90033-5, 1977.
- 18 Saha, A. K., Gupta, R. P., and Arora, M. K.: GIS-based Landslide Hazard Zonation in the Bhagirathi (Ganga) Valley,
19 Himalayas, *International Journal of Remote Sensing*, 23, 357-369, doi: 10.1080/01431160010014260, 2010.
- 20 Saito, H., Nakayama, D., and Matsuyama, H.: Comparison of landslide susceptibility based on a decision-tree model and
21 actual landslide occurrence: The Akaishi Mountains, Japan, *Geomorphology*, 109, 108-121, doi:
22 10.1016/j.geomorph.2009.02.026, 2009.
- 23 Sato, H. P., Hasegawa, H., Fujiwara, S., Tobita, M., Koarai, M., Une, H., and Iwahashi, J.: Interpretation of landslide
24 distribution triggered by the 2005 Northern Pakistan earthquake using SPOT 5 imagery, *Landslides*, 4, 113-122, doi:
25 10.1007/s10346-006-0069-5, 2007.
- 26 Shahabi, H., and Hashim, M.: Landslide susceptibility mapping using GIS-based statistical models and Remote sensing data
27 in tropical environment, *Scientific Reports*, 5, 9899, doi: 10.1038/srep09899, 2015.
- 28 Shrestha, S., Kang, T.-S., and Suwal, M.: An Ensemble Model for Co-Seismic Landslide Susceptibility Using GIS and
29 Random Forest Method, *ISPRS International Journal of Geo-Information*, 6, 365, doi: 10.3390/Ijgi6110365, 2017.
- 30 Siqueira, D. S., Marques, J., Pereira, G. T., Teixeira, D. B., Vasconcelos, V., Carvalho Júnior, O. A., and Martins, E. S.:
31 Detailed mapping unit design based on soil-landscape relation and spatial variability of magnetic susceptibility and soil
32 color, *Catena*, 135, 149-162, doi: 10.1016/j.catena.2015.07.010, 2015.
- 33 Su, C., Wang, L., Wang, X., Huang, Z., and Zhang, X.: Mapping of rainfall-induced landslide susceptibility in Wencheng,
34 China, using support vector machine, *Nat Hazards*, 76, 1759-1779, doi: 10.1007/s11069-014-1562-0, 2015.



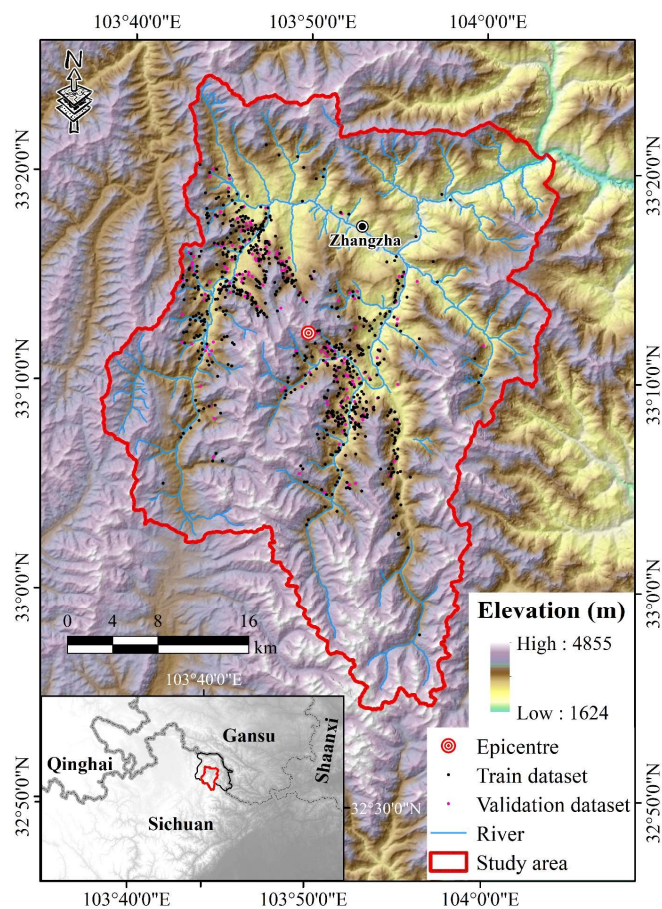
- 1 Tien Bui, D., Pradhan, B., Lofman, O., Revhaug, I., and Dick, O. B.: Landslide susceptibility assessment in the Hoa Binh
- 2 province of Vietnam: A comparison of the Levenberg–Marquardt and Bayesian regularized neural networks,
- 3 *Geomorphology*, 171-172, 12-29, doi: 10.1016/j.geomorph.2012.04.023, 2012.
- 4 Tilmant, A., Vanclooster, M., Duckstein, L., and Persoons, E.: Comparison of fuzzy and nonfuzzy optimal reservoir
- 5 operating policies, *J Water Res Pl-Asce*, 128, 390-398, doi: 10.1061/(ASCE)0733-9496(2002)128:6(390), 2002.
- 6 Umar, Z., Pradhan, B., Ahmad, A., Jebur, M. N., and Tehrani, M. S.: Earthquake induced landslide susceptibility mapping
- 7 using an integrated ensemble frequency ratio and logistic regression models in West Sumatera Province, Indonesia, *Catena*,
- 8 118, 124-135, doi: 10.1016/j.catena.2014.02.005, 2014.
- 9 Vaidya, O. S., and Kumar, S.: Analytic hierarchy process: An overview of applications, *European Journal of Operational*
- 10 *Research*, 169, 1-29, doi: 10.1016/j.ejor.2004.04.028, 2006.
- 11 van Westen, C. J., Castellanos, E., and Kuriakose, S. L.: Spatial data for landslide susceptibility, hazard, and vulnerability
- 12 assessment: An overview, *Engineering Geology*, 102, 112-131, doi: 10.1016/j.enggeo.2008.03.010, 2008.
- 13 Vargas, L. G.: An overview of the analytic hierarchy process and its applications, *European Journal of Operational Research*,
- 14 48, 2-8, doi: 10.1016/0377-2217(90)90056-H, 1990.
- 15 Wang, J., Jin, W., Cui, Y.-f., Zhang, W.-f., Wu, C.-h., and Alessandro, P.: Earthquake-triggered landslides affecting a
- 16 UNESCO Natural Site: the 2017 Jiuzhaigou Earthquake in the World National Park, China, *Journal of Mountain Science*, 15,
- 17 1412-1428, doi: 10.1007/s11629-018-4823-7, 2018a.
- 18 Wang, W., Chen, H., Xu, A. H., and Qu, M. H.: Analysis of the disaster characteristics and emergency response of the
- 19 Jiuzhaigou earthquake, *Nat Hazard Earth Sys*, 18, 1771-1783, doi: 10.5194/nhess-18-1771-2018, 2018b.
- 20 Xu, C., Dai, F. C., Xu, X. W., and Lee, Y. H.: GIS-based support vector machine modeling of earthquake-triggered landslide
- 21 susceptibility in the Jianjiang River watershed, China, *Geomorphology*, 145, 70-80, doi: 10.1016/j.geomorph.2011.12.040,
- 22 2012a.
- 23 Xu, C., Xu, X. W., Dai, F. C., and Saraf, A. K.: Comparison of different models for susceptibility mapping of earthquake
- 24 triggered landslides related with the 2008 Wenchuan earthquake in China, *Computers & Geosciences*, 46, 317-329, doi:
- 25 10.1016/j.cageo.2012.01.002, 2012b.
- 26 Yalcin, A.: GIS-based landslide susceptibility mapping using analytical hierarchy process and bivariate statistics in Ardesen
- 27 (Turkey): Comparisons of results and confirmations, *Catena*, 72, 1-12, doi: 10.1016/j.catena.2007.01.003, 2008.
- 28 Youssef, A. M., Pradhan, B., Jebur, M. N., and El-Harbi, H. M.: Landslide susceptibility mapping using ensemble bivariate
- 29 and multivariate statistical models in Fayfa area, Saudi Arabia, *Environmental Earth Sciences*, 73, 3745-3761, doi:
- 30 10.1007/s12665-014-3661-3, 2015.
- 31 Zhang, G., Cai, Y., Zheng, Z., Zhen, J., Liu, Y., and Huang, K.: Integration of the Statistical Index Method and the Analytic
- 32 Hierarchy Process technique for the assessment of landslide susceptibility in Huizhou, China, *Catena*, 142, 233-244, doi:
- 33 10.1016/j.catena.2016.03.028, 2016.



- 1 Zhao, B., Wang, Y.-s., Luo, Y.-h., Li, J., Zhang, X., and Shen, T.: Landslides and dam damage resulting from the Jiuzhaigou
- 2 earthquake (8 August 2017), Sichuan, China, Royal Society Open Science, 5, 171418, doi: 10.1098/rsos.171418, 2018.
- 3 Zhou, S. H., Chen, G. Q., Fang, L. G., and Nie, Y. W.: GIS-Based Integration of Subjective and Objective Weighting
- 4 Methods for Regional Landslides Susceptibility Mapping, Sustainability, 8, 334, doi: 10.3390/Su8040334, 2016.
- 5 Zhu, A. X., Wang, R. X., Qiao, J. P., Qin, C. Z., Chen, Y. B., Liu, J., Du, F., Lin, Y., and Zhu, T. X.: An expert knowledge-
- 6 based approach to landslide susceptibility mapping using GIS and fuzzy logic, Geomorphology, 214, 128-138, doi:
- 7 10.1016/j.geomorph.2014.02.003, 2014.
- 8

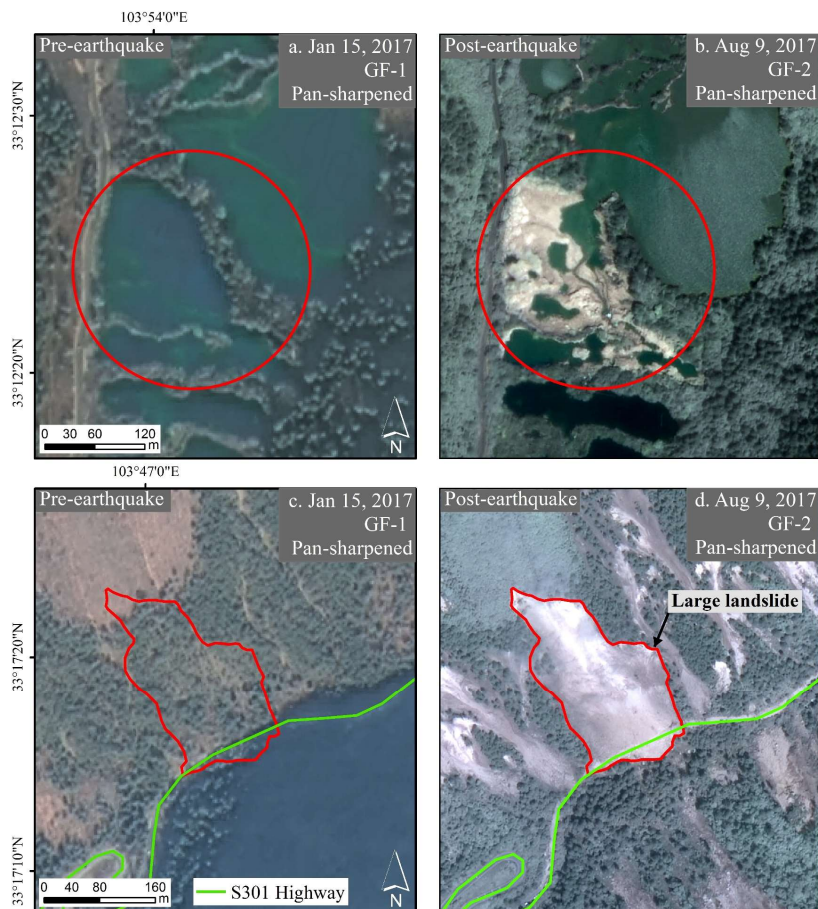


1 Figures



2

3 **Figure 1: The digital map showing the location, topography, river networks, epicentre of the Jiuzhaigou earthquake, as well as the**
4 **locations of earthquake-triggered landslides for training and validation over the study area.**



1
2
3
4
5
6
7
8
9
10

Figure 2: Remote sensing interpretation for earthquake disaster of the study area. a) 2 m spatial resolution GF-1 remotely sensed image acquired on January 15, 2017 before the earthquake compared with b) 1 m spatial resolution GF-2 remotely sensed image acquired on August 9, 2017 after the earthquake, clearly revealed the dried up of the Sparkling Lake after the Jiuzhaigou earthquake; c) 2 m spatial resolution GF-1 remotely sensed image acquired on January 15, 2017 before the earthquake compared with d) 1 m spatial resolution GF-2 remotely sensed image acquired on August 9, 2017 after the earthquake, illustrated the damage of the S301 highway in the Jiuzhaigou earthquake.

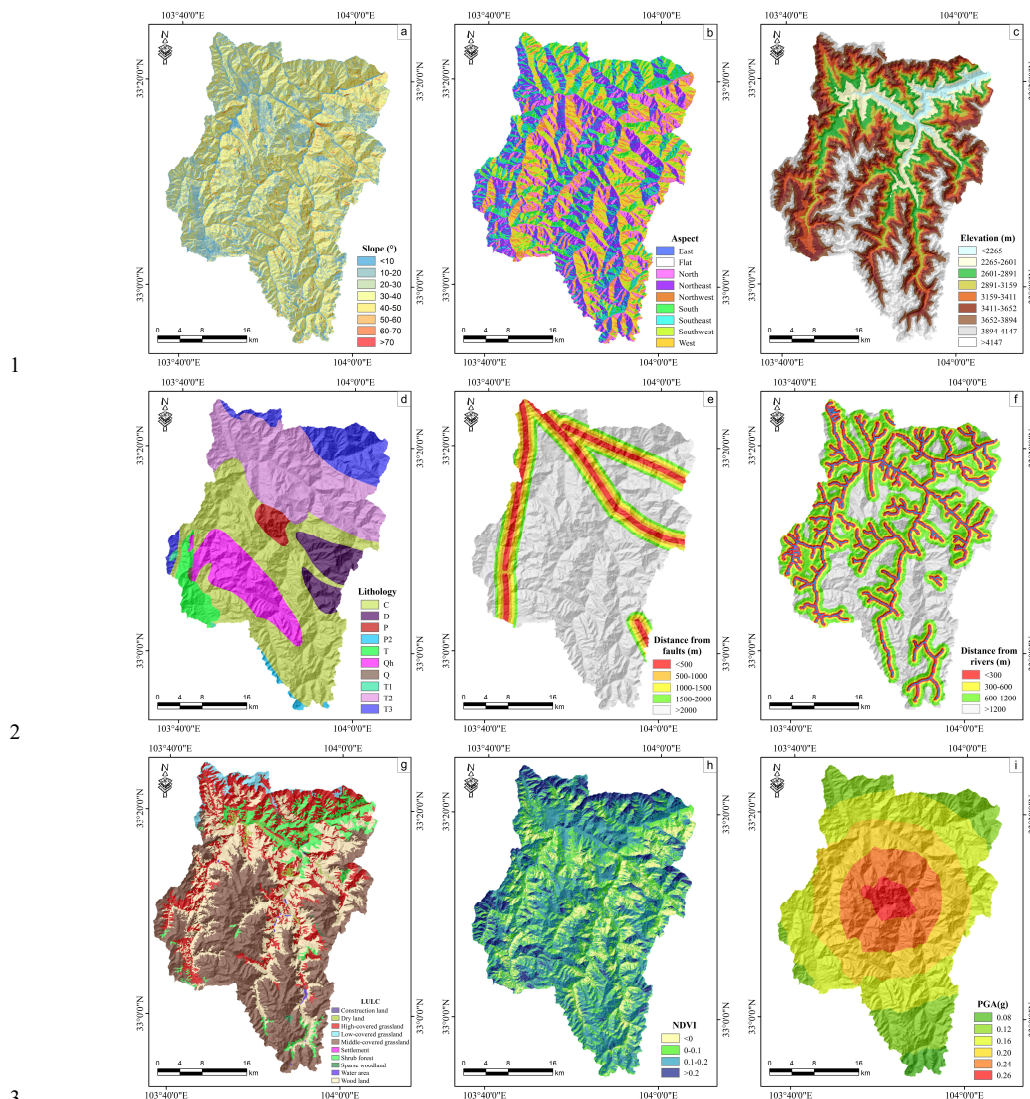
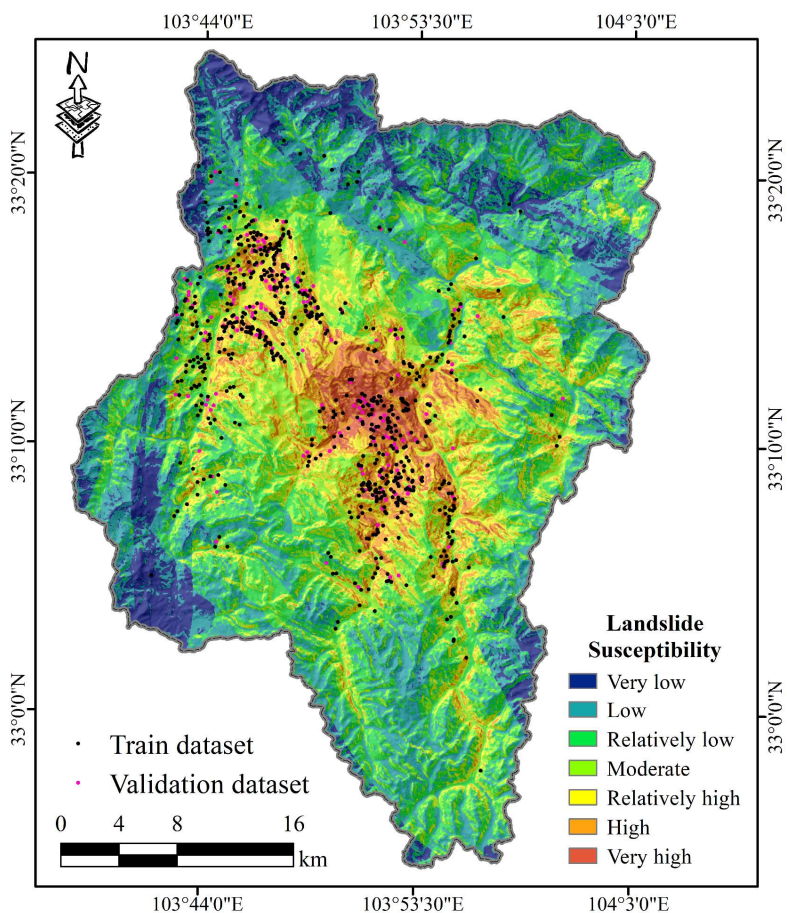
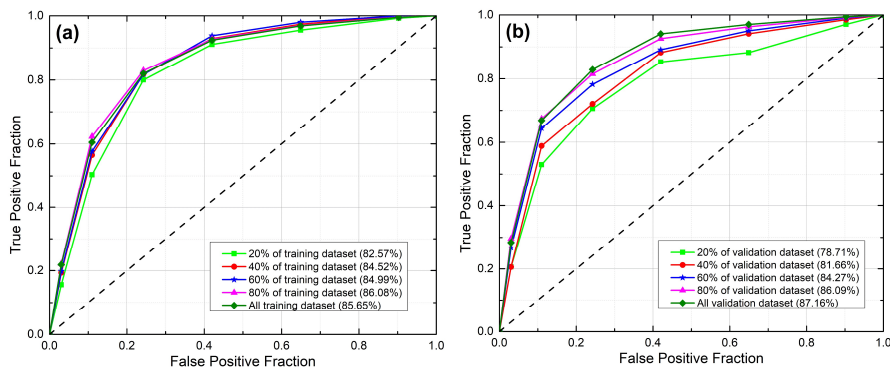


Figure 3: Landslide controlling factor layers used for landslide susceptibility mapping in the study area. (a) Slope, (b) Aspect, (c) Elevation, were all extracted from DEM data, (d) Lithology, digitized from the geological map at 1: 500,000 scale, (e) Distance from faults, calculated by ArcGIS 10.2 software, (f) Distance from rivers, calculated by ArcGIS 10.2 software, (g) LULC, collected from the Geographical Information Monitoring Cloud Platform, (h) NDVI, extracted from the Landsat-8 image, (i) PGA, downloaded from the USGS website.



1
2
3

Figure 4: Landslide susceptibility map of the study area generated by using the integrated weighted index model.



1
2
3
4
5

Figure 5: ROC curves of the Jiuzhaigou landslide susceptibility assessment. (a) Fitting performance of the integrated weighted index model; (b) Prediction performance of the integrated weighted index model.



1 **Tables**

2 **Table 1: Data layers of the study area.**

Data layer	Data format	Scale/resolution	Data source
DEM	Grid	30 m	Shuttle Radar Topography Mission (SRTM)
Sentinel-2A	IMAGINE image	10 m	European Space Agency
Landsat-8	IMAGINE image	30 m	United States Geological Survey (USGS)
GF-1/2	IMAGINE image	2 m/1 m	China Centre for Resources Satellite Data and Application
Lithology	Shapefile (polygon)	1:500,000	The geological map
Fault	Shapefile (line)	1: 500,000	China Earthquake Administration
River	Shapefile (line)	1:10,000	Remote sensing interpretation
LULC	Grid	30 m	Geographical Information Monitoring Cloud Platform
PGA	Shapefile (polygon)	1:25,000	United States Geological Survey (USGS)

3

4

5

6 **Table 2: The pair-wise comparison matrix, factor weights, and consistency ratio obtained in present study.**

Factor	a ₁	a ₂	a ₃	a ₄	a ₅	a ₆	a ₇	a ₈	a ₉	Weight
Elevation (a ₁)	1	1/4	2	1/3	1/4	1	1/3	1/2	2	0.058
Slope (a ₂)		1	4	2	1	3	2	3	4	0.222
Aspect (a ₃)			1	1/3	1/4	1/2	1/3	1/2	1	0.043
Lithology (a ₄)				1	1/2	1	1/2	2	3	0.116
Distance from faults (a ₅)					1	2	1	3	4	0.197
LULC (a ₆)						1	1/2	1	2	0.083
PGA (a ₇)							1	2	3	0.158
Distance from rivers (a ₈)								1	2	0.080
NDVI (a ₉)									1	0.043
Consistency Ratio: 0.017										

7

8



1 **Table 3: The FR and weights for landslide controlling factors for the study area.**

Factor	Class	FR	Weight	Factor	Class	FR	Weight
Slope (°)	<10	0.000	0.222	Elevation(m)	<2265	0.451	0.058
	10-20	0.106			2265-2601	1.153	
	20-30	0.431			2601-2891	2.411	
	30-40	1.270			2891-3159	2.437	
	40-50	2.330			3159-3411	1.496	
	50-60	2.807			3411-3652	0.819	
	60-70	1.804			3652-3894	0.177	
Aspect	>70	0.000	0.043	Lithology	3894-4147	0.021	0.116
	Flat	0.000			>4147	0.000	
	N	1.305			T3	0.030	
	NE	1.116			T2	0.528	
	E	1.662			P	3.431	
	SE	1.343			C	1.819	
	SE	0.965			D	0.544	
	SW	0.590			P2	0.000	
	W	0.646			T	0.039	
	NW	0.560			T1	0.000	
Distance from faults (m)	N	0.819	0.197	Distance from rivers (m)	Qh	0.471	0.080
	<500	0.689			Q	0.000	
	500-1000	0.482			<300	1.302	
	1000-1500	0.594			300-600	1.162	
	1500-2000	0.606			600-1200	0.795	
NDVI	>2000	1.169	0.043	LULC	>1200	0.863	0.083
	<0	1.211			Dry land	0.796	
	0-0.1	1.199			Wood land	2.085	
	0.1-0.2	0.975			Shrub forest	0.164	
PGA (g)	>0.2	0.306	0.158	Sparse woodland	0.000		
	0.08	0.000		Water area	0.970		
	0.12	0.009		High-covered grassland	1.072		
	0.16	0.273		Medium-covered grassland	0.550		
	0.20	1.448		Low-covered grassland	0.000		
	0.24	2.194		Settlement	0.000		
	0.26	3.578		Construction	0.000		

2
3



1 **Table 4: Landslide susceptibility levels and density of landslides in the study area.**

Susceptibility level	Area (km ²)	Percentage of area	Number of landslide occurrences	Percentage of number	Density (no./km ²)
Very Low	130.81	9.72 %	4	0.47 %	0.03
Low	340.86	25.34 %	22	2.61 %	0.06
Relatively low	308.29	22.92 %	35	4.16 %	0.11
Moderate	238.84	17.76 %	89	10.57 %	0.37
Relatively high	178.52	13.27 %	172	20.43 %	0.96
High	107.20	7.97 %	325	38.60 %	3.03
Very High	40.67	3.02 %	195	23.16 %	4.79
Total	1345.19	100 %	842	100 %	--

2